JPET Fast Forward. Published on September 27, 2022 as DOI: 10.1124/jpet.122.001256
This article has not been copyedited and formatted. The final version may differ from this version.

Title Page

A Physiologically-Based Pharmacokinetic Model of the Brain Considering Regional Lipid Variance

Andrew McPherson Heitman, Robert R. Bies, Sorell L. Schwartz

Affiliations:

AMH –Department of Pharmacology and Physiology, Georgetown University Medical Center, Washington, DC

RB - Department of Pharmaceutical Sciences, State University of New York at Buffalo, Buffalo, NY

SLS - Department of Pharmacology and Physiology, Georgetown University Medical Center, Washington, DC

JPET Fast Forward. Published on September 27, 2022 as DOI: 10.1124/jpet.122.001256
This article has not been copyedited and formatted. The final version may differ from this version.

Running Title Page
Region-specific PBPK model of the CNS

Corresponding Author:

Sorell L. Schwartz, Ph.D.
Department of Pharmacology & Physiology
Georgetown University Medical Center
3900 Reservoir Rd, NW
Washington, DC 20057
Mobile (301) 651-6141
sschwa01@georgetown.edu

Number of text pages:12
Number of tables: 10
Number of figures: 5
Number of references: 52
Word counts:
Abstract: 202
Introduction: 675
Discussion: 798
Nonstandard abbreviations used:

AUC	Area under the curve
$AUC_{0-\infty}$	AUC from time zero to infinity
AUC_{0-24}	AUC from time zero to 24 hours
BBB	Blood-brain barrier
BCM	Brain cell membrane
BCSFB	Blood-CSF barrier
C_{max}	Maximal concentration
CNS	Central nervous system
CP	Choroid plexus
CSF	Cerebral spinal fluid
ECF	Extracellular fluid
GM	Grey matter
LMFE	Log mean-fold error
NCA	Noncompartmental analysis
PBPK	Physiologically based pharmacokinetic
PK	Pharmacokinetic
ROB	Rest of brain
ROI	Region of interest
SAS	Subarachnoid space
T_{max}	Time to maximal concentration
WM	White matter
WPBPK	Whole body PBPK

Recommended section assignment: Other

JPET Fast Forward. Published on September 27, 2022 as DOI: 10.1124/jpet.122.001256
This article has not been copyedited and formatted. The final version may differ from this version.

Abstract: Modeling and simulation of the central nervous provides a tool for understanding and predicting the distribution of small molecules throughout the brain tissue and cerebral spinal fluid (CSF) and these efforts often rely on empirical data to make predictions of distributions to move towards a better *mechanistic* understanding. A physiologically based pharmacokinetic (PBPK) model presented here incorporates multiple means of drug distribution to assemble a model for understanding potential factors that may determine the distribution of drugs across various regions of the brain, including both intra- and extracellular regions. Two classes of parameters are presented, the first concerns regional gross anatomical variability of the brain; the second concerns estimation of unbound fractions of drugs using know membrane phospholipid heterogeneity derived from regional lipid content. The model was then tested by comparing its outcomes to data from published human pharmacokinetic studies of acetaminophen, morphine, and phenytoin. The alignment of model predictions in the plasma, CSF, and tissue concentrations with the published data from studies of those three drugs suggests that the model can be a template for identifying drug localization in the brain. Clearly, knowledge of differentiated drug distribution in the brain is a requisite step in postulating pharmacodynamic and certain disease mechanisms.

Significance statement: The application of heterogenous lipid distribution in brain tissue to predict regional variations in drug distribution in the brain via a mathematical model, thus expanding upon the current understanding of mechanisms of drug distribution in the central nervous system.

JPET Fast Forward. Published on September 27, 2022 as DOI: 10.1124/jpet.122.001256
This article has not been copyedited and formatted. The final version may differ from this version.

Introduction

Mathematical modeling in biological sciences spans a range of purpose – from the goal of predicting outcomes to understanding parameter relationships in a biological system(Bies *et al.*, 2008). Semi-physiological or non-physiological *empirical models* apply statistical methods to better describe observed data without necessarily providing intimate mechanistic details of the system; the data modeled determine the structure and parameters of the model. On the other hand, *systems-models* rely on detailing mechanisms quantitatively and testing the outcomes to assess the chosen parameters relationships in the systems where a model structure and parameters are determined *a priori.* Empirical models *describe* data and variations while systems models *create* novel data. Systems-models can broaden understanding of CNS biology interconnectivity and dynamics by incorporating multiple, often isolated mechanisms into a single comprehensive mathematical model. The novel predictions of drug distribution represent an outcome that allows for the testing of the overall system moving the concept of modeling well beyond simply describing data as in the empirical models. As such, the perspective represented by model becomes its own hypothesis and is tested through simulation.

Understanding and predicting drug distribution in the human central nervous system (CNS) is limited by a lack of available tools to observe drug concentrations *in situ*. Pre-clinical animal and cell models provide useful information by integrating wide-ranging individual mechanisms affecting drug distribution into a formal and quantified knowledge. However, the direct translation of these learnings to humans is problematic. The capacity to determine drug disposition in specific brain regions, both intracellularly and extracellularly is no doubt a means to crucial information on disease processes and treatment modalities. In humans, the relationship between neurological disorders and drug distribution localized within the CNS remains elusive. One obvious and overarching reason is limited access to the CNS for fluid and tissue samples. Accordingly, human-based mechanistic modeling is requisite wherein it that can provide a means for extensive hypothesis testing and eventual extrapolation of individual and population dynamics.

The goal of this research is not to test a model per se. An *empirical* modeling effort produces an objective function and p-values to determine model fit with a "final model" presented to describe observed data. In the systems-model, there is a process of developing where different parameters are considered in different arrays for a

stated specific purpose. While each rendering of a "CNS model" may have the same overall goal (describing drug distribution), the specific purpose is more informative. Here we propose a version of a CNS model describing drug distribution in the CNS using a physiologically-based pharmacokinetic (PBPK) model. A PBPK model uses differential equations to describe the drug flux in various compartments representing tissue in the human body allowing simultaneous calculation of tissue specific concentrations over a set period. The subsequent comparison of the simulations to observed data tests the hypothesis presented, in essence asking, "are the mechanisms and processes utilized in the model sufficient to explain drug distribution?" The specific hypothesis presented here vis-à-vis the PBPK model is based on two core components: 1) differential membrane permeability across regions of interest (ROI) and 2) differential unbound concentrations in the brain tissue. These areas of focus are described through the assembly of parameters taken from multiple literature sources that individually have been shown to have *some* impact on pharmacokinetics in the CNS. These parameters are then assembled into a cohesive set of equations represented by the PBPK model and the model is then compared to observed data.

In this research we describe the determination of parameters of interest in the construction of the PBPK model, outline the construction of the system of equations with relevant parameters, simulate the distribution of three drugs with observed data available, and compare the simulation outcomes to the clinical data for each drug. Importantly, all parameters in the model were assembled from data and research unrelated to the test articles and observed data. Ultimately, we demonstrate that the parameters chosen, as described in materials and methods, can reproduce observed data, suggesting that the PBPK model can function as a method for understand drug distribution in the CNS.

JPET Fast Forward. Published on September 27, 2022 as DOI: 10.1124/jpet.122.001256
This article has not been copyedited and formatted. The final version may differ from this version.

Materials and methods

Model development began with a whole-body PBPK (WBPBPK) model to provide the input to the CNS portions of the model. A published WBPBPK model was chosen from the literature as a starting point (Jones and Rowland-Yeo, 2013) for the structural components of the current model. The total number of compartments was reduced to limit the overall dimensionality of the model while maintaining equations and parameters that were shown to be impactful in replicating plasma concentrations as determined by iterative simulations of a generic parameter set. No formal lumping process was used. Ordinary differential equations were used to describe the flux into each compartment of the WBPBPK model. The distribution of clearances and absorption rates (when necessary) were estimated from existing literature. Partition coefficients for the WBPBPK were derived using Rowland and Rodgers methods(Rodgers *et al.*, 2005; Rodgers and Rowland, 2006a) and computed utilizing programming and a unified tissue database from literature (Utsey *et al.*, 2020). Structural parameters for the WBPBPK were taken from literature and are presented in the Supplemental Section I: Model Specifications, table 1.

The goal of the parameterization of the model was to capture the differences in the CNS regions related to membrane permeability and unbound fractions. With regards to membrane permeability the BBB, BCSFB, and cellular membranes of the CNS were all considered. The first set of parameters determined were the passive flux of drug in the brain tissue and CSF. Two main barriers are involved the permeability of a drug into the CNS, the blood-CSF barrier (BCSFB) and the blood-brain barrier (BBB). The BBB is in the capillaries of the brain and is comprised of endothelial cells connected via tight junctions while the BCSFB is formed by the epithelial cells of the choroid plexus (CP) (Redzic, 2011). The epithelial cells comprising the BCSFB reside in the ventricles of the brain and is relatively more permeable than the BBB as one of the CP's major functions in the brain is fluid homeostasis(Solár *et al.*, 2020). Active transporters at the BBB and BCSFB add more complexity due to the uneven distribution of various transporters and, maybe, differing function (efflux vs. influx). They are not a focus of this model but are addressed through the addition of a general term representing observed ratios due to active transport for each specific drug (Lange, 2004; Löscher and Potschka, 2005; Bendayan *et al.*, 2006; Lange *et al.*, 2018; Billington *et al.*, 2019). To address this complexity, the regions of the CNS that receive drug input across the BBB and BCSFB were parameterized in a way that reflects the known differences.

JPET Fast Forward. Published on September 27, 2022 as DOI: 10.1124/jpet.122.001256
This article has not been copyedited and formatted. The final version may differ from this version.

The first step in addressing these differences for the CNS portion of the model was to split a generic CNS compartment from the WBPBPK model into separate CSF and brain tissue compartments as shown in figure 2. Passive permeability was estimated via the application of permeability-surface area products where the clearance of drug across either the BBB or the BCSFB is a product of the flow of blood, the surface area available for permeation, and the permeability of the substance (Crone, 1963; Pardridge, 2016). Blood flow values for each region of the brain were taken from literature and estimated as a fraction of total cardiac output to scale with body weight. The barrier permeability for each drug tested was determined according to Yamamoto(Yamamoto, Välitalo, Berg, *et al.*, 2017) for the BBB, BCSFB, the brain cell membrane (BCM).

All four cerebral ventricles are represented by a single compartment to capture the entire surface area of the CP available for passive permeability and due to the complex and uneven distribution of the CP amongst the four ventricles (Solár *et al.*, 2020). Additionally, the combination of all four ventricles into a single compartment facilitates the scaling of the CP with body weight without any arbitrary fractioning between the lateral and third and fourth ventricles. Representing the CP accurately is a key component of the model and helps to distinguish the BBB from the BCSFB. The basal cisterns function as a transfer compartment as there is no drug exchange occurring in this compartment and serves as a conduit to the subarachnoid space (SAS) of the spine. The SAS of the spine is the site of drug reabsorption from the CSF.

Three regions of the brain were chosen with a fourth generic rest-of-brain (ROB) compartment. These regions of interest (ROI) were further divided into a microvasculature component, extracellular component, intracellular component, and phagolysosome compartment. Microvasculature represents the capillary beds that are the main site of BBB transfer(Pardridge, 2020), the extracellular environment represents the milieu surrounding brain parenchyma, the intracellular component represents a generic characterization of parenchymal cells in the brain, and the phagolysosomal space represents the estimated sum of low pH vacuoles in the cytosol of a brain cell. Anatomical parameters for the brain tissue were taken from imaging data and are listed in the supplemental materials with the values for the CSF compartments. The parameters used in the CNS compartments are found in Supplemental Section I: Model Specifications, tables 2-5 and Supplemental Section III: Determining Regional Lipophilicity, tables 6 and 7.

JPET Fast Forward. Published on September 27, 2022 as DOI: 10.1124/jpet.122.001256
This article has not been copyedited and formatted. The final version may differ from this version.

The second component tested in the model was the estimation of free fraction of drug. Estimation of the free fraction of drug in each of the regions of the brain tissue was accomplished by 1) estimating the lipid/phospholipid distribution for each region 2) calculating the fraction unbound based upon the lipid/phospholipid distribution, and 3) applying the ionization fraction differences based on the drugs pKa and the regional pH (this is incorporated into the free drug calculations as described in Supplemental II. Estimating Binding Fraction). Neutral and acidic phospholipids are unevenly distributed between the intracellular and extracellular environment; most specifically, charged and uncharged phospholipids are heterogeneously distributed between the internal and external lamina of cell membranes(Devaux, 1991). The distribution of phospholipids was estimated for each ROI and separated by intra and extracellular portions by utilizing relative fractions of white matter (WM) and grey matter (GM) as well as the stoichiometry between internal and external facing phospholipids(O'Brien and Sampson, 1965; Kwee and Nakada, 1988). We adapted the methods for determining partitioning coefficients used in the WBPBPK and applying the estimated distribution of phospholipids, drug specific binding and partitioning is estimated for each region of the microvasculature(Rodgers and Rowland, 2006b; a; Rodgers *et al.*, 2007). The parameters for the distribution of phospholipids are found in Supplemental III. Determining Regional Lipophilicity, tables 6 and 7.

Models were written into C++ files for simulation via the MRGsolve package (Elmokadem *et al.*, 2019; Alhadab and Brundage, 2020) on RStudio v1.2.5019 running R v4.0. Once the model model was established, the parameters were assembled into the C++ file and any calculated variables added to the drug specific modeling code. The conceptual alignment of the modeling interactions is shown in figure 1. The coding development was comprised of three steps and at each step layers of complexity were added. Initially WBPBPK model was adapted from Jones 2013 (Jones and Rowland-Yeo, 2013) with a generic CNS compartment as shown in figure 2. Second, the CNS compartments were added. Third, the brain tissue was broken into regions of interest and separated into four spaces each – microvasculature, extracellular space, intracellular space, and phagolysosomal space. At each step mass balance was monitored as a quality control measure. All equations used are found in supplemental Section IV: PBPK Equations. All coding and data used in this publication can be found at the link provided in Supplemental V: Code and Data.

Drug specific parameters (table 1) were entered into the model prior to simulation. A normal distribution for any parameter with known physiological variation (e.g., rate of absorption; total body clearance) was created and

JPET Fast Forward. Published on September 27, 2022 as DOI: 10.1124/jpet.122.001256
This article has not been copyedited and formatted. The final version may differ from this version.

sampled prior to each simulation when a distribution of parameters was available. The number of virtual subjects (N) input for each model simulation reflects the specific study used for model assessment's overall N and all demographics available (e.g., body weight) were input into the model prior to each simulation run. The model is simulated between 500-1000 times for the given N and the outputs amalgamated into a single data set. This dataset was then analyzed for fit per the method below and compared to literature values of either individual time point or reported descriptive PK statistics, depending on availability. Model outputs for observed data in the CSF, plasma, or tissue were assessed by calculating the log mean-fold error (LMFE). The LMFE for a time-point or PK parameter is calculated as (Peters, 2008):

$$LMFE = 10^{[\frac{1}{n}\sum \log(FE)]}$$

Where the *FE* is the fold-error or ratio of the individual prediction-observation points such that it is always ≥ 1, and *n* is the number of comparisons for the time point or parameter. Typically, the acceptable fold-error for predictions is 2.0; however, it is an arbitrary number that might not capture the true variability in an observed population, but it is sufficient for the purpose of model evaluation (Abduljalil *et al.*, 2014). Time-point level data was extract from a publication, when possible, via WebPlot Digitizer-4.3 (https://automeris.io/WebPlotDigitizer/)(Drevon *et al.*, 2017).

When observable data for intracellular and extracellular concentrations was not available, relative concentrations from the published literature were used in testing the behavior of the model system. The ratios between simulated concentrations in various brain regions, including microanatomy, were computed from data output for each region. A range of AUC ratios between the regions (0.8-1.2) was chosen *a priori* range to allow for a qualitative assessment of equivalence between the regions compared. While the absolute concentrations are available for these simulations, they are not informative with regards to the objective of this research. Extracellular and intracellular $AUC_{0\text{-}24}$ was computed for each virtual subject in each simulation and compared to across regions. Extracellular and intracellular concentrations were also compared *within* each region to estimate the variability between the extracellular and intracellular space.

JPET Fast Forward. Published on September 27, 2022 as DOI: 10.1124/jpet.122.001256
This article has not been copyedited and formatted. The final version may differ from this version.

Results

All three modules of the model (WBPBPK, CSF, brain tissue including sub-compartments) were tested using drugs selected based on the availability of literature that contained information about simultaneous plasma and CSF or tissue data. This allowed the validation of the regions of the CNS that were selected to be put in context of the plasma concentrations. The data available were then compared to the predictions as described in the previous section. Results shown compare pharmacokinetic parameters, time-series data, or both when available. The drugs selected serve as a means for testing the parameter sets.

Acetaminophen was used to test the model performance in predicting simultaneous plasma and CSF concentrations utilizing two studies. In Singla (Singla *et al.*, 2012), three groups of between 6 and 7 subjects received one of either oral (1000 mg), IV (1000 mg over 15 minutes), or rectal (not examined here) acetaminophen. Simultaneous plasma and CSF were collected via catheter over 6 hours. In Langford (Langford *et al.*, 2016), three groups of subjects received either oral (1000 mg or 1500 mg) or IV (1000 mg over 20 minutes) and both plasma and CSF were collected over 6 hours. Study parameters were modeled after the demographics of each study and simulations were run according to table 8. Mean time-series data from the Singla study are compared to the 95 per cent prediction interval in figure 3. Both the oral and IV simulations of plasma administration of acetaminophen met acceptability criteria in the time-series and non-compartmental analysis (NCA) comparisons as shown in table 1. The corresponding CSF analysis (figure 3 and table 1) displayed an acceptable fit in both the oral and IV simulations as well as for the NCA statistics, while the time-series met acceptability only in the oral simulation. The discrepancy in the early phase of the CSF data from patients receiving IV acetaminophen can arise from multiple factors including a small sample number in the clinical study, sampling errors in the early collection portion and model limitations.

NCA statistics were compared in the Langford study for all dose groups. The data are presented in table 2. The model neared acceptability criteria in all three studies of morphine plasma concentrations. The LMFE were all outside of the acceptability criteria from the CSF. However, in those, the model-generated CSF ranges for each statistic analyzed were similar. Notably, the observed patient data from the Langford study showed wide variations in concentration profiles between patients and that contributed to mean values not adequately representing the

JPET Fast Forward. Published on September 27, 2022 as DOI: 10.1124/jpet.122.001256
This article has not been copyedited and formatted. The final version may differ from this version.

individual patient data. This, alone or in combination with model limitations, is likely reflected in the model output for CSF.

Human studies with morphine were used to examine extracellular predictions in the cortex via two studies dealing with three patients with traumatic brain injury(Bouw *et al.*, 2001; Ederoth *et al.*, 2004). All three patients received 10 mg IV morphine over 10 minutes and samples were collected via microdialysis from extracellular fluid (ECF). Plasma samples were also collected intermittently for all three subjects. Demographic data were combined with literature data and body weight from the studies (Ball *et al.*, 2012). Model simulations were compared to the observed plasma and the ECF data as shown in figure 4. The plasma predictions showed a LMFE of 1.788 over all time points when comparing the 50^{th} percentile predicted values to the observed values reported in literature. The model-generated ECF concentration in cortex was compared to the "better brain" sections as described in the observed data (Bouw *et al.*, 2001; Ederoth *et al.*, 2004). The LMFE over all time points for the ECF was 1.394.

Phenytoin was used to test the model performance in predicting plasma, CSF, and brain tissue drug content. Wilder assessed phenytoin in four groups of patients with status epilepticus (Wilder *et al.*, 1977). For the first group, the kinetics of a single IV infusion of phenytoin was assessed. The second group was studied to determine the efficacy of IV phenytoin (no PK samples collected); for the third group, consecutive plasma and CNS tissue samples were collected for PK analysis; and in the fourth group, drug in plasma and spinal fluid was assessed. Tissue samples were taken from areas of "normal" brain during tumor extraction via craniotomy. Time series data were reported along with demographics and dosing information for each individual subject. Plasma samples were collected for each group and aligned with CSF and tissue samples. The demographic and dosing information was used as data input for simulation. All patient plasma values fell within the acceptance criteria as shown in figure 5. Plasma and CSF concentrations for patients in the third group are shown in figure 5 as well and while the LMFE of the plasma data are within the acceptance criteria, the simulated CSF data fall outside. One possibility for this is likely reflected in the apparent under-prediction in the early phase of the plasma infusion as shown in figure which may cause both a lag in T_{max} as well as a shortfall in C_{max}. Both plasma and tissue concentrations fall within the acceptance criteria for the fourth group of patients (figure 5).

A comparison of predicted extracellular concentrations across regions of the brain are show in tables 1-7. All regions were compared to one another, and the resulting ratios listed in the tables. Acetaminophen and Morphine

showed equivalent distribution between regions of the brain (in both extracellular and intracellular regions). Phenytoin showed a higher concentration of drug in regions of the brain with a greater white matter concentration aligning with some empirical evidence that demonstrated higher concentrations in more lipid rich regions(Goldberg and Crandall, 1978; Rambeck *et al.*, 1992). A comparison of each region intra- versus extra-cellular predicted concentrations are shown in tables 8-10. Acetaminophen showed a significantly higher exposure in the intracellular environment aligning with described mechanisms of action(Jóźwiak-Bebenista and Nowak, 2014). Similarly, morphine showed a significantly higher drug concentration in the extracellular environment aligning with the known pharmacology (Trescot *et al.*, 2008; Sverrisdóttir *et al.*, 2015). Phenytoin was equivalent between extra- and intra-cellular spaces.

JPET Fast Forward. Published on September 27, 2022 as DOI: 10.1124/jpet.122.001256
This article has not been copyedited and formatted. The final version may differ from this version.

Discussion

Mathematical models of complex human biology necessarily need to be "fit-for-purpose". Adhering to the adage coined by George Box(Box, 1976) "all models are wrong, some are useful", a mathematical model of the CNS is bound to be "wrong", but if the design reflects *specific* research questions it can provide useful information. Here we have aimed to look at the integration of lipid heterogeneity in combination with regional physiological differences on the impact of heterogenous drug distribution in brain tissue. We have demonstrated that this approach aligns with observable data and known mechanisms of action of the drugs used in the referenced studies and, as such, the model presented here can be a tool in further explorations of drug distribution in neurological diseases affecting the selected regions and the impact of pathology on these regions.

Recent models of the CNS address several similar parameters and approaches in the current model, as is expected. Yamamoto et al(Yamamoto, Välitalo, Berg, *et al.*, 2017; Yamamoto, Välitalo, Huntjens, *et al.*, 2017; Y Yamamoto *et al.*, 2018) extrapolated regional CNS distribution of drugs from rats to humans by estimating the passive permeability derived from drug properties in the brain. In their models the tissue was partitioned into an extracellular intracellular, and lysosomal sections while still treating the brain as one homogenous tissue. Incorporated CSF compartments were used to capture drug diffusion from brain tissue to CSF as well as the permeability of the BCSFB. A key component of the Yamamoto models is the estimation of permeability by incorporating *in vitro* data(Avdeef *et al.*, 2004; Grumetto *et al.*, 2016) to determine the passive permeability across the BBB, BCSFB, as well as the cell and lysosomal membranes. Zakaria *et al*(Zakaria and Badhan, 2018) developed a model in rat and human that divided the CNS into specific regions of the brain, namely the hippocampus and the frontal cortex. The Zakaria model incorporated observed permeabilities from literature, corrected for the surface area of the BBB in each region, to estimate the variation between the nuclei. Both modeling efforts marked significant progress in understanding CNS drug distribution mechanisms. However, the Zakaria model relies on *drug* specific empirical evidence to estimate the regional distribution while the Yamamoto models treat the brain tissue as a single homogenous entity. All these prior models are informative, and the current effort is intended add to that information The goal of the modeling efforts presented here is fit to purpose: understand the potential impact of regional morphology on drug distribution.

JPET Fast Forward. Published on September 27, 2022 as DOI: 10.1124/jpet.122.001256
This article has not been copyedited and formatted. The final version may differ from this version.

While much of the discussion is focused on the tissue concentrations, the relationship between CSF and tissue is also of importance. The CSF concentrations served as a surrogate in clinical studies for some time but unfortunately, they are not always representative of what is happening in the ECF, let alone the intracellular environment due to a litany of reasons and has been well discussed elsewhere (Shen *et al.*, 2004; Pardridge, 2016; Saleh *et al.*, 2021). However, a model that can represent the mechanistic differences in drug permeability can provide useful insight into the relationship between CSF concentration and brain tissue concentration. The clinical access to the CSF provides an important tool in the assessment of CNS targeted therapeutics and a "human-to-human" translation of CSF drug concentration to brain concentration, at an individual level, can prove important information with regards to factors affecting variability. Similarly, the narrow range of variation in AUC of the ECF and ICF predictions indicates that a relatively wide plasma concentration can be associated with brain content and distribution that do not reflect the width of plasma concentrations. Often in clinical trials, human plasma concentration is used as a surrogate for brain tissue concentrations and the resulting variability is used to describe a variation in pharmacodynamics (PD). While in certain cases, this might be true – but the results here indicate that a simple approach (comparing plasma concentrations to PD outcomes) is limited in its utility.

The results of this research present evidence that two main factors determining regional drug distribution in the CNS, including cellular and subcellular distribution, are related to CNS barrier permeability and phospholipid heterogeneity of a generic brain cell *together*. In instances where *direct* observations are unavailable to confirm model predictions, we have relied on *indirect* evidence that the qualitative distribution is representative. In the instance of acetaminophen and morphine, as mentioned in the results, the relative ratios of distribution are indicative of the target-effect described in literature. A qualitative description is utilized here to focus on the limited ability of observing these concentrations *in vivo* so far. Presenting the absolute concentrations without the ability to compare or confirm may lead to inappropriate assumptions about the feasibility of the model. The current model represents a modality for understanding the effect of regional variations on drug distribution in the brain.

JPET Fast Forward. Published on September 27, 2022 as DOI: 10.1124/jpet.122.001256
This article has not been copyedited and formatted. The final version may differ from this version.

References

Abduljalil K, Cain T, Humphries H, and Rostami-Hodjegan A (2014) Deciding on Success Criteria for Predictability of Pharmacokinetic Parameters from In Vitro Studies: An Analysis Based on In Vivo Observations. *Drug Metab Dispos* 42:1478–1484.

Alhadab AA, and Brundage RC (2020) Physiologically-Based Pharmacokinetic Model of Sertraline in Human to Predict Clinical Relevance of Concentrations at Target Tissues. *Clin Pharmacol Ther* 108:136–144.

Avdeef A, Nielsen P, and pharmaceutical T-O journal of (2004) PAMPA—a drug absorption in vitro model: 11. Matching the in vivo unstirred water layer thickness by individual-well stirring in microtitre plates.

Ball K, Bouzom F, Scherrmann J-M, Walther B, and Declèves X (2012) Development of a Physiologically Based Pharmacokinetic Model for the Rat Central Nervous System and Determination of an In Vitro–In Vivo Scaling Methodology for the Blood–Brain Barrier Permeability of Two Transporter Substrates, Morphine and Oxycodone. *J Pharm Sci* 101:4277–4292.

Bendayan R, Ronaldson PT, Gingras D, and Bendayan M (2006) In Situ Localization of P-glycoprotein (ABCB1) in Human and Rat Brain. *J Histochem Cytochem* 54:1159–1167.

Bies R, Gastonguay M, and Schwartz S (2008) Mathematics for Understanding Disease. *Clinical Pharmacology & Therapeutics* 83:904–908.

Billington S, Salphati L, Hop CECA, Chu X, Evers R, Burdette D, Rowbottom C, Lai Y, Xiao G, Humphreys WG, Nguyen TB, Prasad B, and Unadkat JD (2019) Interindividual and Regional Variability in Drug Transporter Abundance at the Human Blood–Brain Barrier Measured by Quantitative Targeted Proteomics. *Clin Pharmacol Ther* 106:228–237.

Bouw R, Ederoth P, Lundberg J, Ungerstedt U, Nordstrom C-H, and Hammarlund-Udenaes M (2001) Increased blood-brain barrier permeability of morphine in a patient with severe brain lesions as determined by microdialysis. *Acta Anaesth Scand* 45:390–392.

Box GEP (1976) Science and Statistics. *Journal of the American Statistical Association* 71:791–799.

Crone C (1963) The Permeability of Capillaries in Various Organs as Determined by Use of the 'Indicator Diffusion' Method. *Acta Physiol Scand* 58:292–305.

Devaux PF (1991) Static and dynamic lipid asymmetry in cell membranes. *Biochemistry-us* 30:1163–1173.

Drevon DD, Fursa SRS, and Malcolm ALA (2017) Intercoder Reliability and Validity of WebPlotDigitizer in Extracting Graphed Data. *Behavior modification* 41:323–339.

Ederoth P, Tunblad K, Bouw R, Lundberg CJF, Ungerstedt U, Nordström C, and Hammarlund-Udenaes M (2004) Blood–brain barrier transport of morphine in patients with severe brain trauma. *Brit J Clin Pharmaco* 57:427–435.

Elmokadem A, Riggs MM, and Baron KT (2019) QSP and PBPK Modeling with mrgsolve: A Hands-on Tutorial. *Cpt Pharmacometrics Syst Pharmacol*, doi: 10.1002/psp4.12467.

Goldberg MA, and Crandall PH (1978) Human brain binding of phenytoin. *Neurology* 28:881–881.

Grumetto L, Russo G, and Barbato F (2016) Immobilized Artificial Membrane HPLC Derived Parameters vs PAMPA-BBB Data in Estimating in Situ Measured Blood–Brain Barrier Permeation of Drugs. *Molecular Pharmaceutics* 13:2808–2816.

Jones H, and Rowland-Yeo K (2013) Basic Concepts in Physiologically Based Pharmacokinetic Modeling in Drug Discovery and Development. *CPT: Pharmacometrics & Systems Pharmacology* 2:1–12.

Jóźwiak-Bebenista M, and Nowak JZ (2014) Paracetamol: mechanism of action, applications and safety concern. *Acta Pol Pharm* 71:11–23.

Kwee IL, and Nakada T (1988) Phospholipid profile of the human brain: 31P NMR spectroscopic study. *Magnet Reson Med* 6:296–299.

Lange ECM de (2004) Potential role of ABC transporters as a detoxification system at the blood–CSF barrier. *Adv Drug Deliver Rev* 56:1793–1809.

Lange ECMD, Berg DJ vd, Bellanti F, Voskuyl RA, and Syvänen S (2018) P-glycoprotein protein expression versus functionality at the blood-brain barrier using immunohistochemistry, microdialysis and mathematical modeling. *Eur J Pharm Sci* 124:61–70.

Langford RA, Hogg M, Bjorksten AR, Williams DL, Leslie K, Jamsen K, and Kirkpatrick C (2016) Comparative Plasma and Cerebrospinal Fluid Pharmacokinetics of Paracetamol After Intravenous and Oral Administration. *Anesthesia Analgesia* 123:610–615.

Liu T, Ivaturi V, and Gobburu J (2019) Integrated Model to Describe Morphine Pharmacokinetics in Humans. *J Clin Pharmacol* 59:1070–1077.

Löscher W, and Potschka H (2005) Role of drug efflux transporters in the brain for drug disposition and treatment of brain diseases. *Prog Neurobiol* 76:22–76.

O'Brien JS, and Sampson EL (1965) Lipid composition of the normal human brain: gray matter, white matter, and myelin. *J Lipid Res* 6:537–44.

Ouzzine M, Gulberti S, Ramalanjaona N, Magdalou J, and Fournel-Gigleux S (2014) The UDP-glucuronosyltransferases of the blood-brain barrier: their role in drug metabolism and detoxication. *Front Cell Neurosci* 8:349.

Pardridge WM (2016) CSF, blood-brain barrier, and brain drug delivery. *Expert Opin Drug Del* 13:963–975.

Pardridge WM (2020) The Isolated Brain Microvessel: A Versatile Experimental Model of the Blood-Brain Barrier. *Front Physiol* 11:398.

Peters SA (2008) Evaluation of a Generic Physiologically Based Pharmacokinetic Model for Lineshape Analysis. *Clin Pharmacokinet* 47:261–275.

Polasek TM, Polak S, Doogue MP, Rostami-Hodjegan A, and Miners JO (2009) Assessment of inter-individual variability in predicted phenytoin clearance. *Eur J Clin Pharmacol* 65:1203.

Rambeck B, Schnabel R, May T, Jürgens U, and Villagràn R (1992) Postmortem Concentrations of Phenytoin in Different Regions of the Brain and in the Serum. *Ther Drug Monit* 14:27–35.

Redzic Z (2011) Molecular biology of the blood-brain and the blood-cerebrospinal fluid barriers: similarities and differences. *Fluids Barriers Cns* 8:3.

Rodgers T, Leahy D, and pharmaceutical R-M of (2005) Physiologically based pharmacokinetic modeling 1: predicting the tissue distribution of moderate-to-strong bases. , doi: 10.1002/jps.20322.

Rodgers T, Leahy D, and Rowland M (2007) Rodgers T, Leahy D, Rowland M. 2005. Physiologically based pharmacokinetic modeling 1: Predicting the tissue distribution of moderate-to-strong bases. J Pharm Sci 94:1259–1276. *Journal of Pharmaceutical Sciences* 96:3151–3152.

Rodgers T, and Rowland M (2006a) Physiologically based pharmacokinetic modelling 2: Predicting the tissue distribution of acids, very weak bases, neutrals and zwitterions. *Journal of Pharmaceutical Sciences* 95:1238–1257.

Rodgers T, and Rowland M (2006b) Physiologically based pharmacokinetic modelling 2: Predicting the tissue distribution of acids, very weak bases, neutrals and zwitterions. *J Pharm Sci* 95:1238–1257.

Saleh MAA, and Lange ECM de de (2021) Impact of CNS Diseases on Drug Delivery to Brain Extracellular and Intracellular Target Sites in Human: A "WHAT-IF" Simulation Study. *Pharm* 13:95.

Saleh MAA, Loo CF, Elassaiss-Schaap J, and Lange ECMD (2021) Lumbar cerebrospinal fluid-to-brain extracellular fluid surrogacy is context-specific: insights from LeiCNS-PK3.0 simulations. *J Pharmacokinet Phar* 1–17.

Sechi G, Petruzzi V, Rosati G, Tanca S, Monaco F, Formato M, Rubattu L, and Riu PD (1989) Brain Interstitial Fluid and Intracellular Distribution of Phenytoin. *Epilepsia* 30:235–239.

Shen D, Artru A, and reviews A-K drug delivery (2004) Principles and applicability of CSF sampling for the assessment of CNS drug delivery and pharmacodynamics.

Singla NK, Parulan C, Samson R, Hutchinson J, Bushnell R, Beja EG, Ang R, and Royal MA (2012) Plasma and Cerebrospinal Fluid Pharmacokinetic Parameters After Single-Dose Administration of Intravenous, Oral, or Rectal Acetaminophen. *Pain Pract* 12:523–532.

Solár P, Zamani A, Kubíčková L, Dubový P, and Joukal M (2020) Choroid plexus and the blood–cerebrospinal fluid barrier in disease. *Fluids Barriers Cns* 17:35.

Sverrisdóttir E, Lund TM, Olesen AE, Drewes AM, Christrup LL, and Kreilgaard M (2015) A review of morphine and morphine-6-glucuronide's pharmacokinetic–pharmacodynamic relationships in experimental and clinical pain. *Eur J Pharm Sci* 74:45–62.

Trescot AM, Datta S, Lee M, and Hansen H (2008) Opioid pharmacology. *Pain Physician* 11:S133-53.

Utsey K, Gastonguay MS, Russell S, Freling R, Riggs MM, and Elmokadem A (2020) Quantification of the Impact of Partition Coefficient Prediction Methods on PBPK Model Output Using a Standardized Tissue Composition. *Drug Metab Dispos* dmd.120.090498.

Walker MC, Alavijeh MS, Shorvon SD, and Patsalos PN (1996) Microdialysis Study of the Neuropharmacokinetics of Phenytoin in Rat Hippocampus and Frontal Cortex. *Epilepsia* 37:421–427.

Wilder BJ, Ramsay RE, Willmore LJ, Feussner GF, Perchalski RJ, and Shumate JB (1977) Efficacy of intravenous phenytoin in the treatment of status epilepticus: Kinetics of central nervous system penetration. *Ann Neurol* 1:511–518.

Yamamoto Y, Välitalo P, and of … W-Y (2018) Prediction of human CNS pharmacokinetics using a physiologically-based pharmacokinetic modeling approach.

Yamamoto Y, Välitalo PA, Berg D-J van den, Hartman R, Brink W van den, Wong YC, Huntjens DR, Proost JH, Vermeulen A, Krauwinkel W, Bakshi S, Aranzana-Climent V, Marchand S, Dahyot-Fizelier C, Couet W, Danhof M, Hasselt JGC van, and Lange ECM de (2017) A Generic Multi-Compartmental CNS Distribution Model Structure for 9 Drugs Allows Prediction of Human Brain Target Site Concentrations. *Pharmaceutical Research* 34:333–351.

Yamamoto Y, Välitalo PA, Huntjens DR, Proost JH, Vermeulen A, Krauwinkel W, Beukers MW, Berg D van den, Hartman R, Wong YC, Danhof M, Hasselt JGC van, and Lange ECM de (2017) Predicting Drug Concentration-Time Profiles in Multiple CNS Compartments Using a Comprehensive Physiologically-Based Pharmacokinetic Model. *CPT: Pharmacometrics & Systems Pharmacology* 6:765–777.

Yamamoto Yumi, Välitalo PA, Wong Y, Huntjens DR, Proost JH, Vermeulen A, Krauwinkel W, Beukers MW, Kokki H, Kokki M, Danhof M, Hasselt J van, and Lange E de (2018) Prediction of human CNS pharmacokinetics using a physiologically-based pharmacokinetic modeling approach. *European Journal of Pharmaceutical Sciences* 112.

Zakaria Z, and Badhan R (2018) Development of a Region-Specific Physiologically Based Pharmacokinetic Brain Model to Assess Hippocampus and Frontal Cortex Pharmacokinetics. *Pharmaceutics* 10:14.

JPET Fast Forward. Published on September 27, 2022 as DOI: 10.1124/jpet.122.001256
This article has not been copyedited and formatted. The final version may differ from this version.

Authorship contributions:

Participated in research design: Andrew M. Heitman, Robert R. Bies, Sorell L. Schwartz

Performed data analysis: Andrew M. Heitman

Wrote or contributed to the writing of the manuscript: Andrew M. Heitman, Robert R. Bies, Sorell L. Schwartz

Footnotes:

Contents of this paper were submitted to Georgetown University School of Graduate Studies by AMH in partial fulfillment of the degree of Doctor of Philosophy

While no human studies were directly conducted during the course of this research, all cited data presented here from published studies in humans were, to our knowledge, collected ethically and in line with published guidance documents.

This work received no external funding.

None of the authors have an actual or perceived conflict of interest with the contents of this article.

JPET Fast Forward. Published on September 27, 2022 as DOI: 10.1124/jpet.122.001256
This article has not been copyedited and formatted. The final version may differ from this version.

Legends for figures

1. Overview of model development and module interaction. One of the aims of the entire model is to be able to simultaneously predict time-concentration profiles in each compartment and model the relationship between the input and output of drug flow between the selected areas. The plasma model serves sole as a means for replicating observed drug concentrations that would be expected to contribute to both sub-models contained in the CNS model.

2. (clockwise from bottom left): Schematic of full body PBPK model. The CNS modules (both CSF and tissue models) are represented as a singular compartment for the sake of illustration. Expansion of CNS model including CSF and Brain Tissue portions: MV=microvasculature supplying region; ECF= extracellular fluid; ICF=intracellular fluid; SAS=subarachnoid space; ROB=rest of brain Clbbb,in = Clearance from microvasculature across BBB into ECF; Clbbb,out = Clearance from the ECF to the MV; Clbcm,in= clearance from ECF to ICF, CLbcm,out=clearance from ICF to ECF; Cllyso,in=clearance from ICF across phagolysosomal membrane; Clyso,out=clearance from phagolysosomal compartment to ICF. Model of drug distribution in microanatomy of the tissue including microvasculature: Qart=blood flow from the artery; Qvein=blood flow to the vein; Fb/i=Fraction bound and ionized; Qecf=ECF flow out from interstitial area to the CSF; Fion=fraction ionized

3. Acetaminophen validation: Black dots represent mean concentration data from the study reported with error bars representing a 35% CV based upon reported data in the study. Solid black line represents the 50th percentile predicted value while the shaded area represents the 95% prediction interval over 1000 simulations of the specified number of subjects. A. Data taken from individual time points for oral administration of 1000 mg of acetaminophen in 7 healthy volunteers. The LMFE for all datapoints shown for the plasma and CSF were 1.61 and 1.524. B. Data taken from individual time points for IV administration of 1000 mg of acetaminophen in 6 healthy volunteers. The LMFE for all datapoints shown for the plasma and CSF were 1.416 and 3.006 respectively.

4. Morphine study in 3 subjects with TBI taken from the non-injured side of the cortex. Dots represent individual time points; Solid line represents the predicted 50th percentile of drug in the ECF; the shaded region represents the 95th percentile of projections. Both log and linear plots are presented. The LMFE for plasma and ECF when comparing all three patients to the 50th percentile model projected value is 1.788 and 1.394, respectively.

5. Phenytoin study in 33 subjects from Wilder. Black dots are observed data points from literature. Black line is 50th percentile value of model predicted drug concentration. Shaded region represents 95th percentile of predicted values. Plasma from all patients is shown in the top row in both Log and linear plots; plasma for all patients when compared to predicted 50th percentile had a LMFE of 1.383. Middle row represents the plasma and CSF values for 6 patients with a LMFE of 1.388 and 2.295 respectively. Bottom row represents the plasma and brain tissue samples from 3 subjects with a LMFE of 1.361 and 1.16 respectively.

JPET Fast Forward. Published on September 27, 2022 as DOI: 10.1124/jpet.122.001256
This article has not been copyedited and formatted. The final version may differ from this version.

Tables and Figures

Drug	Molecular Weight	Log P	pKa	$F_{u,p}$	$F_{u,csf}$	B:P
Acetaminophen (Saleh and Lange, 2021)	151.2	0.91	9.46	0.85	0.991	1
Morphine (Ball *et al.*, 2012; Ouzzine *et al.*, 2014; Yumi Yamamoto *et al.*, 2018; Liu *et al.*, 2019; Saleh and Lange, 2021)	285.3	0.87	10.96	0.65	0.997	1.02
Phenytoin (Polasek *et al.*, 2009; Saleh and Lange, 2021)	252.3	2.28	8.42	0.1	0.995	0.61

Drug	Absorption	Clearance Hepatic	Clearance Renal	Clearance Brain	Transporter Effects	Charge Class
Acetaminophen	15 h^{-1}	22800	780	0	None	Neutral
Morphine	0.139 h^{-1}	30 mL/min/kg	0.11*Hepatic Clearance	0	PGP[a]	Base
Phenytoin	0.632 h^{-1}	16000	121	0	None	Acid

Table 1. Drug properties used in model simulations. a) While the PGP interaction with morphine is well established, all subjects received an unknown dose of fentanyl, a known PGP inhibitor, and the generic asymmetry factor was set to 1.

JPET Fast Forward. Published on September 27, 2022 as DOI: 10.1124/jpet.122.001256
This article has not been copyedited and formatted. The final version may differ from this version.

Extracellular Acetaminophen	*Thalamus*	*Cortex*	*Basal Ganglia*	*Rest of Brain*
Thalamus	X	0.8176-0.8179	0.9833-0.9835	0.9998-1.0006
Cortex	0.8176-0.8179	X	0.8313-0.8317	0.8174-0.8184
Basal Ganglia	0.9833-0.9835	0.8313-0.8317	X	0.9833-0.9839
Rest of Brain	0.9998-1.0006	0.8174-0.8184	0.9833-0.9839	X

Table 2. Comparison of prediction regional extracellular ratios for bioequivalence of acetaminophen. Ranges contained completely outside of 0.8-1.2 are considered non-equivalent.

JPET Fast Forward. Published on September 27, 2022 as DOI: 10.1124/jpet.122.001256
This article has not been copyedited and formatted. The final version may differ from this version.

Intracellular Acetaminophen	*Thalamus*	*Cortex*	*Basal Ganglia*	*Rest of Brain*
Thalamus	X	0.9490-0.9496	1.0772-1.0781	0.9243-0.9245
Cortex	0.9490-0.9496	X	0.8802-0.8815	0.8777-0.8785
Basal Ganglia	1.0772-1.0781	0.8802-0.8815	X	0.9966-0.9966
Rest of Brain	0.9243-0.9245	0.8777-0.8785	0.9966-0.9966	X

Table 3. Comparison of prediction regional intracellular ratios for bioequivalence of acetaminophen. Ranges contained completely outside of 0.8-1.2 are considered non-equivalent.

JPET Fast Forward. Published on September 27, 2022 as DOI: 10.1124/jpet.122.001256
This article has not been copyedited and formatted. The final version may differ from this version.

Extracellular Morphine	*Thalamus*	*Cortex*	*Basal Ganglia*	*Rest of Brain*
Thalamus	X	0.8804-0.8885	1.0621-1.0717	0.9919-0.9981
Cortex	0.8804-0.8885	X	0.8811-0.8928	0.8733-0.8868
Basal Ganglia	1.0621-1.0717	0.8811-0.8928	X	0.9911-0.9932
Rest of Brain	0.9919-0.9981	0.8733-0.8868	0.9911-0.9932	X

Table 4. Comparison of prediction regional extracellular ratios for bioequivalence of morphine. Ranges contained completely outside of 0.8-1.2 are considered non-equivalent

JPET Fast Forward. Published on September 27, 2022 as DOI: 10.1124/jpet.122.001256
This article has not been copyedited and formatted. The final version may differ from this version.

Intracellular **Morphine**	*Thalamus*	*Cortex*	*Basal Ganglia*	*Rest of Brain*
Thalamus	X	0.9729-0.9848	1.0621-1.0717	0.9307-0.9418
Cortex	0.9729-0.9848	X	0.9078-0.9271	0.9055-0.9276
Basal Ganglia	1.0621-1.0717	0.9078-0.9271	X	0.9974-1.0004
Rest of Brain	0.9307-0.9418	0.9055-0.9276	0.9974-1.0004	X

Table 5. Comparison of prediction regional intracellular. ratios for bioequivalence of morphine. Ranges contained completely outside of 0.8-1.2 are considered non-equivalent

JPET Fast Forward. Published on September 27, 2022 as DOI: 10.1124/jpet.122.001256
This article has not been copyedited and formatted. The final version may differ from this version.

Extracellular Phenytoin	*Thalamus*	*Cortex*	*Basal Ganglia*	*Rest of Brain*
Thalamus	X	0.8576-0.8578	1.0764-1.0765	0.9191-0.9194
Cortex	0.8576-0.8578	X	**0.7966-0.7969**	**0.7883-0.7888**
Basal Ganglia	1.0764-1.0765	**0.7966-0.7969**	X	0.9895-0.9897
Rest of Brain	0.9191-0.9194	**0.7883-0.7888**	0.9895-0.9897	X

Table 6. Comparison of prediction regional extracellular ratios for bioequivalence of phenytoin. Ranges contained completely outside of 0.8-1.2 are considered non-equivalent

JPET Fast Forward. Published on September 27, 2022 as DOI: 10.1124/jpet.122.001256
This article has not been copyedited and formatted. The final version may differ from this version.

Intracellular Phenytoin	*Thalamus*	*Cortex*	*Basal Ganglia*	*Rest of Brain*
Thalamus	X	0.8585-0.8587	1.0754-1.0756	0.9197-0.9200
Cortex	0.8585-0.8587	X	**0.7981-0.7985**	**0.7896-0.7901**
Basal Ganglia	1.0754-1.0756	**0.7981-0.7985**	X	0.9893-0.9895
Rest of Brain	0.9197-0.9200	**0.7896-0.7901**	0.9893-0.9895	X

Table 7. Comparison of prediction regional intracellular ratios for bioequivalence of phenytoin. Ranges contained completely outside of 0.8-1.2 are considered non-equivalent

JPET Fast Forward. Published on September 27, 2022 as DOI: 10.1124/jpet.122.001256
This article has not been copyedited and formatted. The final version may differ from this version.

Comparison of extracellular/intracellular concentration - Acetaminophen	
Region	**Intracellular: Extracellular 90% CI Ratio**
Thalamus	**2.8004-2.8501**
Cortex	**3.2514-3.3082**
Basal Ganglia	**3.0677-3.1244**
ROB	**3.0286-3.0827**

Table 8. Comparison of predicted intracellular versus extracellular concentrations of acetaminophen. Rations completely outside of 0.8-1.2 are considered not-equivalent.

JPET Fast Forward. Published on September 27, 2022 as DOI: 10.1124/jpet.122.001256
This article has not been copyedited and formatted. The final version may differ from this version.

Comparison of extracellular/intracellular concentration - Morphine	
Region	**Intracellular:Extracellular 90% CI Ratio**
Thalamus	**0.4518-0.4795**
Cortex	**0.5008-0.5299**
Basal Ganglia	**0.4823-0.5143**
ROB	**0.4788-0.5110**

Table 9. Comparison of predicted intracellular versus extracellular concentrations of morphine. Rations completely outside of 0.8-1.2 are considered not-equivalent.

JPET Fast Forward. Published on September 27, 2022 as DOI: 10.1124/jpet.122.001256
This article has not been copyedited and formatted. The final version may differ from this version.

Comparison of extracellular/intracellular concentration - Phenytoin	
Region	**Extracellular:Intracellular 90% CI Ratio**
Thalamus	1.0171-1.0712
Cortex	1.0181-1.0813
Basal Ganglia	1.0162-1.0163
ROB	1.0164-1.0166

Table 10. Comparison of predicted intracellular versus extracellular concentrations of phenytoin. Rations completely outside of 0.8-1.2 are considered not-equivalent

Figure 1

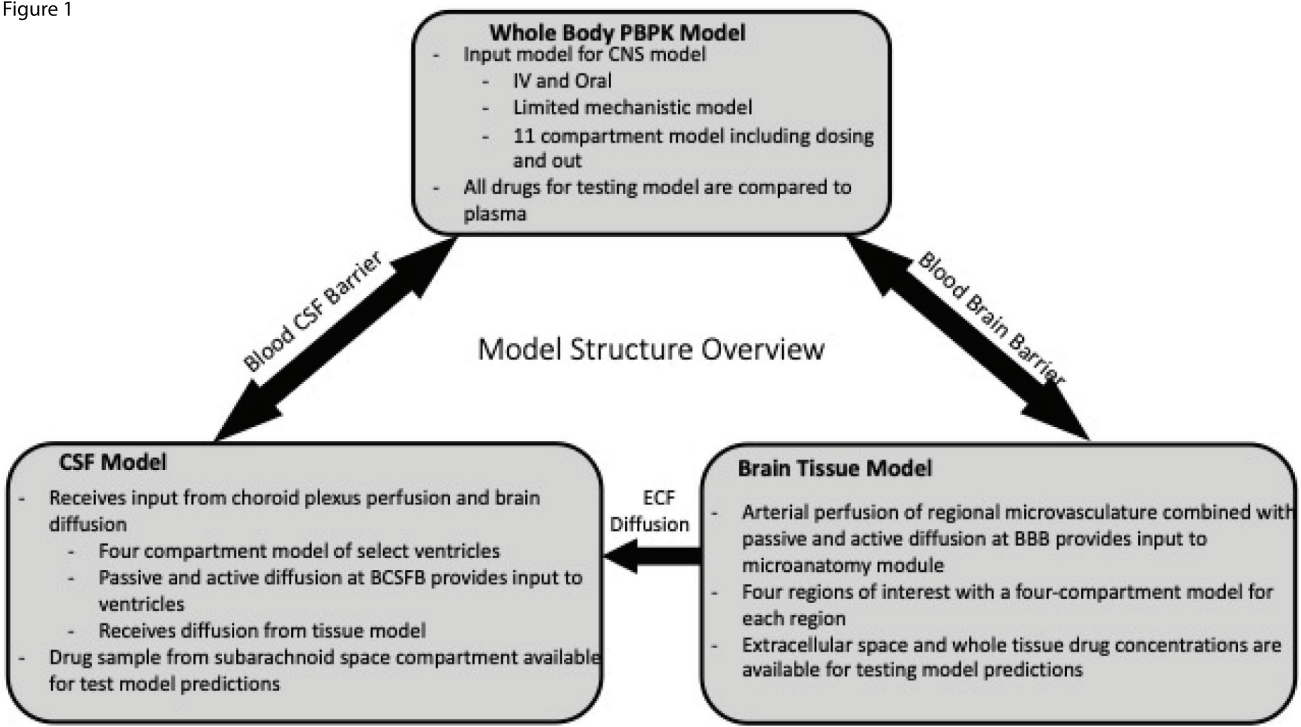
Whole Body PBPK Model
- Input model for CNS model
- IV and Oral
- Limited mechanistic model
- 11 compartment model including dosing and out
- All drugs for testing model are compared to plasma
Blood CSF Barrier
Blood Brain Barrier
Model Structure Overview
CSF Model
- Receives input from choroid plexus perfusion and brain diffusion
- Four compartment model of select ventricles
- Passive and active diffusion at BCSFB provides input to ventricles
- Receives diffusion from tissue model
- Drug sample from subarachnoid space compartment available for test model predictions
ECF Diffusion
Brain Tissue Model
- Arterial perfusion of regional microvasculature combined with passive and active diffusion at BBB provides input to microanatomy module
- Four regions of interest with a four-compartment model for each region
- Extracellular space and whole tissue drug concentrations are available for testing model predictions

Figure 2

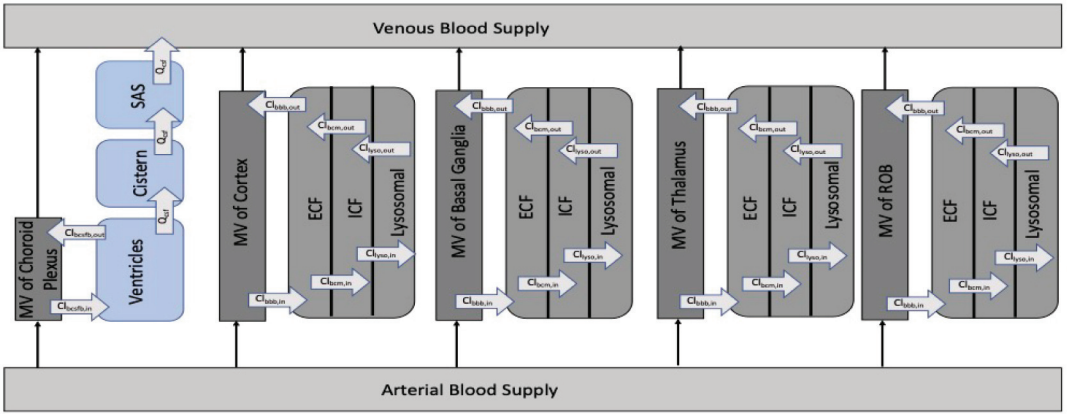
Venous Blood Supply
SAS
Cistern
Ventricles
MV of Choroid Plexus
MV of Cortex
MV of Basal Ganglia
MV of Thalamus
MV of ROB
ECF
ICF
Lysosomal
Arterial Blood Supply

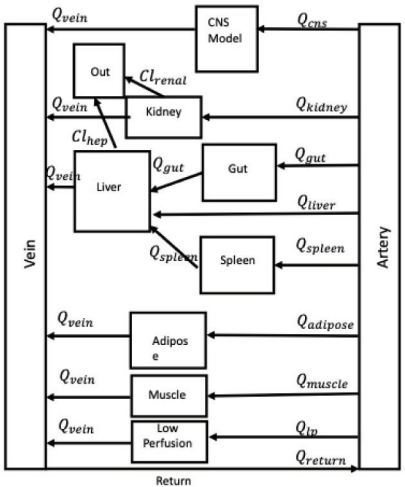
CNS Model
Out
Kidney
Liver
Gut
Spleen
Adipose
Muscle
Low Perfusion
Vein
Artery
Return

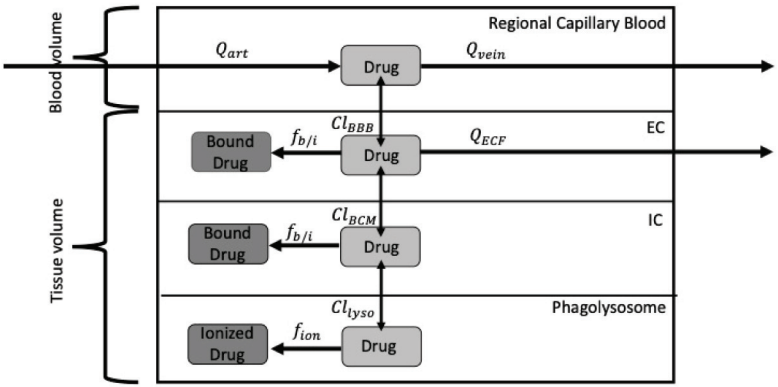
Blood volume
Tissue volume
Regional Capillary Blood
Drug
Bound Drug
Ionized Drug
EC
IC
Phagolysosome

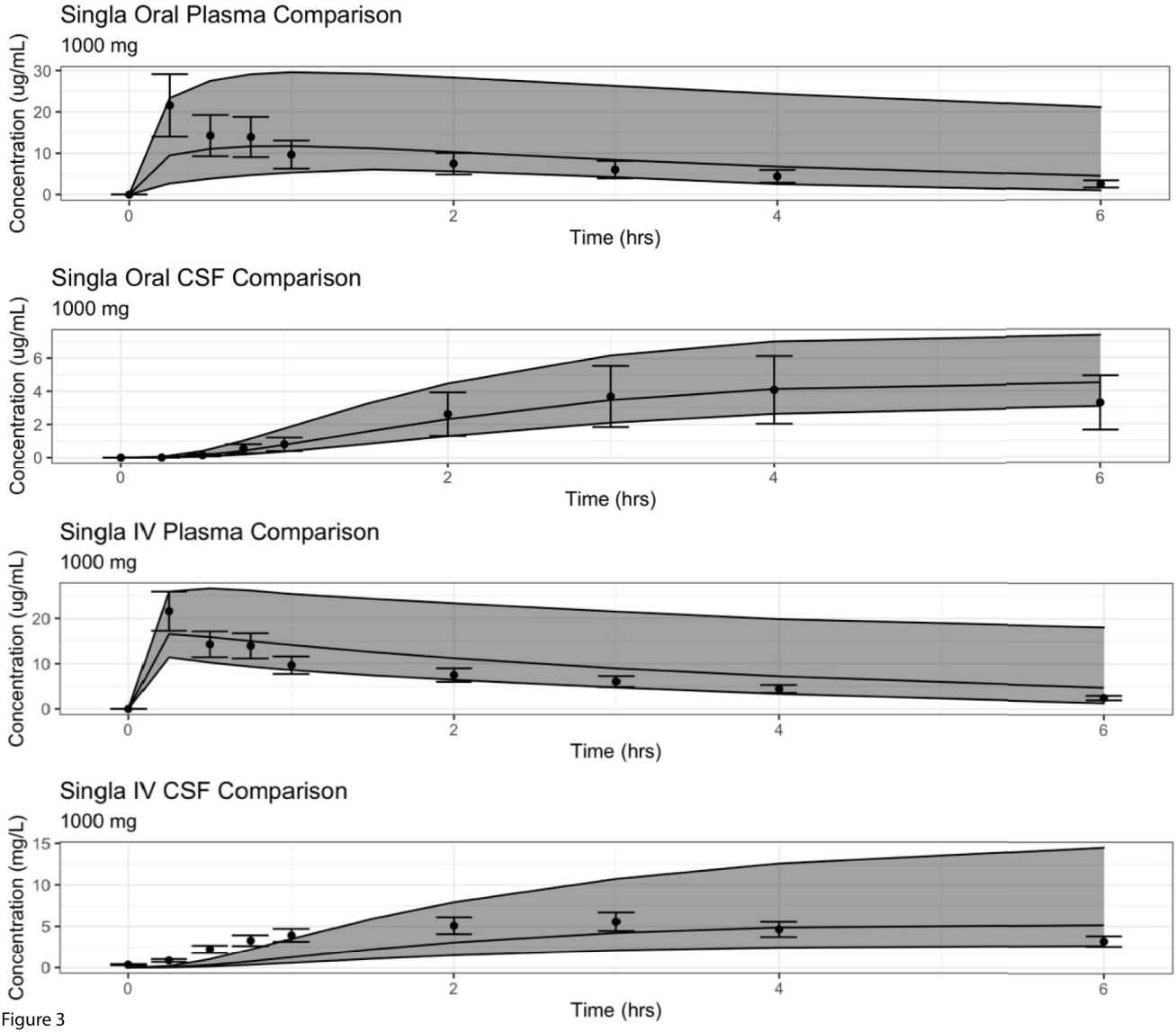
Singla Oral Plasma Comparison
1000 mg
Concentration (ug/mL)
Time (hrs)
Singla Oral CSF Comparison
1000 mg
Concentration (ug/mL)
Time (hrs)
Singla IV Plasma Comparison
1000 mg
Concentration (ug/mL)
Time (hrs)
Singla IV CSF Comparison
1000 mg
Concentration (mg/L)
Time (hrs)

Figure 3

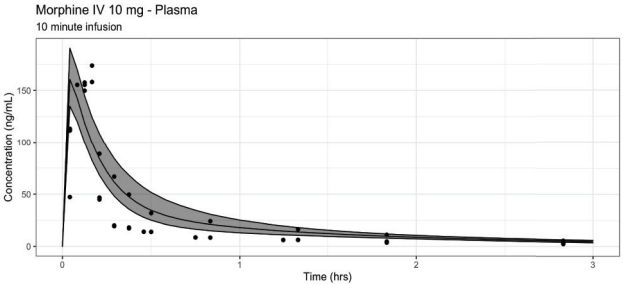
Morphine IV 10 mg - Plasma
10 minute infusion
Concentration (ng/mL)
150
100
50
0
0
1
2
3
Time (hrs)

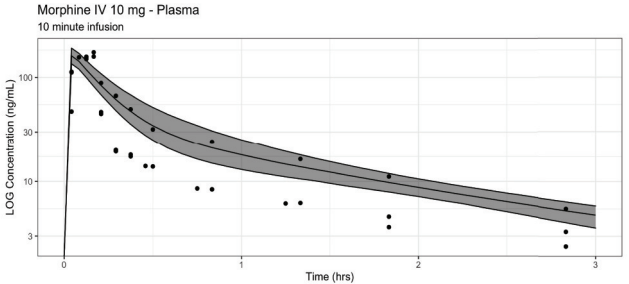
Morphine IV 10 mg - Plasma
10 minute infusion
LOG Concentration (ng/mL)
100
30
10
3
0
1
2
3
Time (hrs)

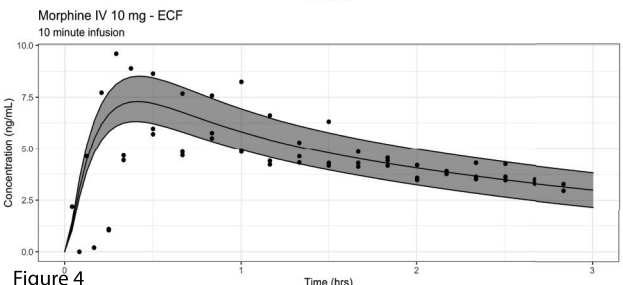
Morphine IV 10 mg - ECF
10 minute infusion
Concentration (ng/mL)
10.0
7.5
5.0
2.5
0.0
0
1
2
3
Time (hrs)

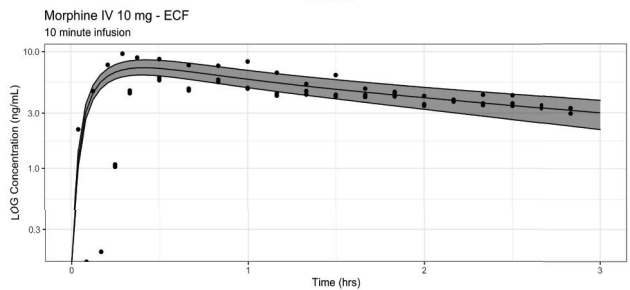
Morphine IV 10 mg - ECF
10 minute infusion
LOG Concentration (ng/mL)
10.0
3.0
1.0
0.3
0
1
2
3
Time (hrs)

Figure 4

Figure 5

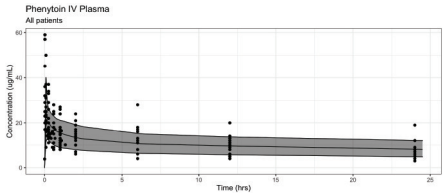
Phenytoin IV Plasma
All patients
Concentration (ug/mL)
Time (hrs)

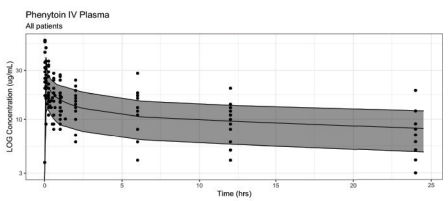
Phenytoin IV Plasma
All patients
LOG Concentration (ug/mL)
Time (hrs)

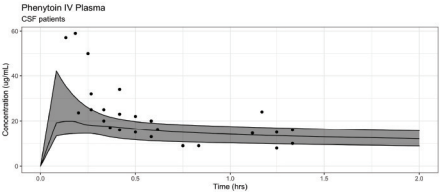
Phenytoin IV Plasma
CSF patients
Concentration (ug/mL)
Time (hrs)

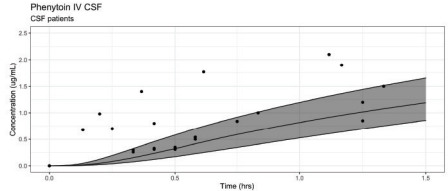
Phenytoin IV CSF
CSF patients
Concentration (ug/mL)
Time (hrs)

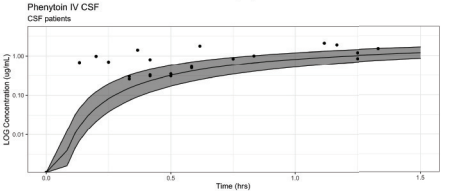
Phenytoin IV CSF
CSF patients
LOG Concentration (ug/mL)
Time (hrs)

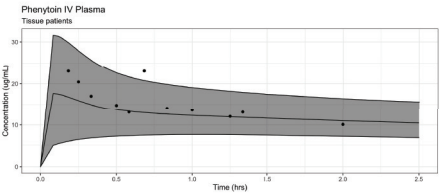
Phenytoin IV Plasma
Tissue patients
Concentration (ug/mL)
Time (hrs)

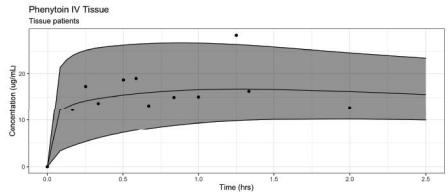
Phenytoin IV Tissue
Tissue patients
Concentration (ug/mL)
Time (hrs)

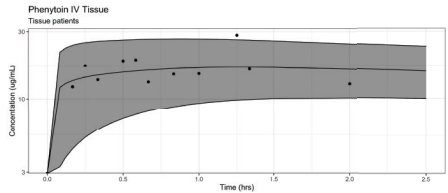
Phenytoin IV Tissue
Tissue patients
Concentration (ug/mL)
Time (hrs)